In-line holographic microscopy with model-based analysis

Caroline Martin [1], Lauren E. Altman[2], Siddharth Rawat [3], Anna Wang [3],
David G. Grier[2] and Vinothan N. Manoharan [1,4] ✉

Abstract | An in-line holographic microscope is an optical microscope outfitted with a coherent light source, such as a laser. Light scattered by the specimen interferes with the transmitted beam, and the intensity of that interference pattern constitutes a hologram. Unlike a conventional photograph, a hologram contains information about the phase of the scattered light that is useful for measuring the composition and 3D arrangement of microscopic objects in the specimen. This Primer presents an overview of experimental methods and discusses three recent analysis techniques: fitting scattering models to the hologram; using machine learning to localize and classify the specimen; and a hybrid approach that uses machine learning to initialize fits. The combination of holographic microscopy and model-based analysis is well suited to applications where precise, quantitative results are needed with high acquisition speed. Such applications include studying properties of heterogeneous colloidal dispersions, measuring colloidal interactions, monitoring stresses in soft materials, detecting molecular binding and aggregation, and following the motion of microorganisms in three dimensions. We discuss the reproducibility and current limitations of each method. Finally, we anticipate directions for future development and provide an outlook on the integration between experiment and computational analysis, an emerging paradigm for microscopy.

Holograms
2D intensity patterns resulting from the interference between light scattered from an object and a reference beam.

[1]Harvard John A. Paulson School of Engineering and Applied Sciences, Harvard University, Cambridge, MA, USA.

[2]Department of Physics and Center for Soft Matter Research, New York University, New York, NY, USA.

[3]School of Chemistry, UNSW Sydney, Sydney, New South Wales, Australia.

[4]Department of Physics, Harvard University, Cambridge, MA, USA.

✉e-mail: vnm@seas.harvard.edu

https://doi.org/10.1038/s43586-022-00165-z

It is not difficult to make a holographic microscope, a microscope that captures holograms rather than photographs. One needs only to replace the white light source in a standard light microscope with a laser aimed at the specimen. The resulting instrument captures in-line holograms[1]. Although the word hologram might evoke images from popular culture, such as projections of Tupac Shakur or Princess Leia, a true hologram is not an image projected in 3D space. Instead, it is a 2D pattern of bright and dark fringes. The fringes of an in-line hologram form when light scattered from the specimen interferes with light transmitted through it, as shown in FIG. 1a.

Compared with a conventional photograph, a hologram such as the example in FIG. 1b can be difficult to interpret by eye. And unlike the vivid, colourful photographs captured by optical microscopy, the monochrome fringes of a hologram are unlikely to grace a journal cover. These concerns raise the question of why anyone would want to convert a microscope into a holographic microscope.

Our answer is that what is important is not the image itself but, instead, what we infer from it. We usually want to do more than just see a microscopic object; we want to precisely quantify its properties — what it is made of, how big it is, where it lies in 3D space and

how fast it moves. This is where holographic microscopy excels. Electromagnetic radiation has both an amplitude and phase, but conventional optical microscopes capture little information about the phase. By contrast, a holographic microscope is designed to capture phase information, which is encoded in the fringes. The phase information allows us to quantify many features of a microscopic specimen. For example, the 3D structure and composition of a specimen can be inferred from a single 2D hologram. Denis Gabor, the inventor of holography, showed that shining light through a recorded hologram generates a 3D reconstruction of the light scattered by the original object[2,3]. Reconstruction has enabled non-invasive 3D imaging of colloidal particles[4–6], material microstructures[7], microorganisms[4,7–10] and living eukaryotic cells[11–13]. More complex optical set-ups can provide additional information about phase changes within a specimen[14–16] and yield tomograms of complex 3D specimens[17,18].

This Primer focuses on an alternative analysis methodology: extracting information directly from the hologram without reconstructing it. The analysis relies on physics-based models of how microscopic objects scatter light. Unlike reconstruction, model-based analysis requires prior information about the object's
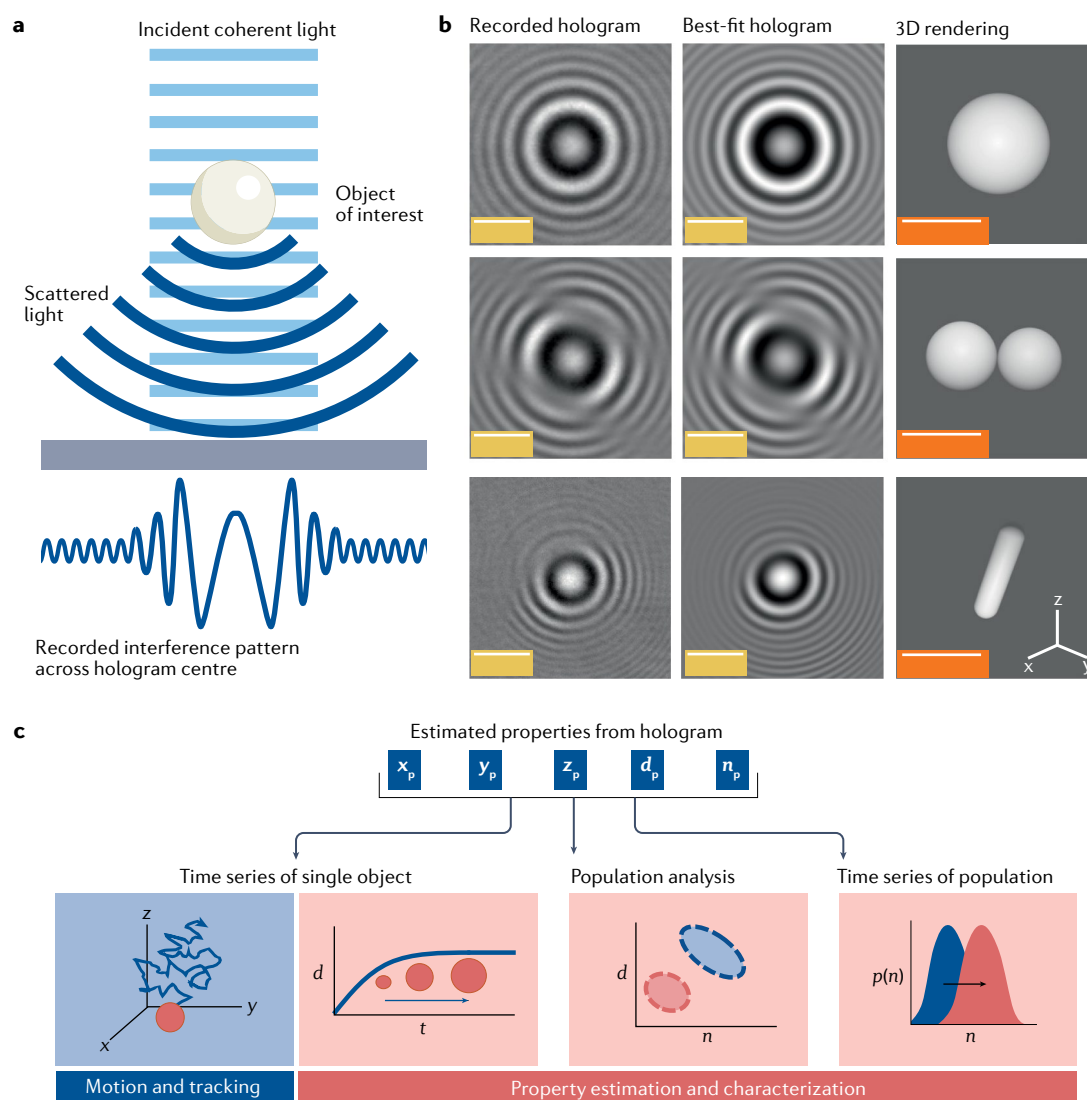
Fig. 1 | **Hologram formation and analysis. a** | Incident coherent light (light blue) interferes with the light scattered (dark blue) by a specimen. Useful information about the specimen can be extracted from the resulting interference pattern, or hologram, shown as the intensity across its centreline. **b** | Holograms, best fits and 3D renderings of a single sphere, sphere doublet and a capsule-shaped bacterium. Best-fit holograms and 3D renderings are generated from the estimated properties of the specimen, including position, diameter and refractive index. **c** | Hologram analysis yields information that is useful for applications. Analysing many holograms from the same object as a function of time can reveal its motion in 3D space or how its properties change. Analysing holograms from a population of objects can differentiate multiple species within a sample. Finally, analysing a hologram from a population of objects over time can reveal changes in the distribution of properties. Yellow scale bars = 5 μm; orange scale bars = 1 μm. d_p, particle's diameter; n_p, particle's refractive index; x_p, y_p and z_p, particle's position. Part **b** (bottom row) adapted with permission from REF.[114], Optica Publishing Group.

Fringes
The bright or dark bands in an image that are produced by the interference of light.

Holographic microscopy
The use of a microscope with a coherent or semi-coherent light source to record holograms of microscopic objects.

Reconstruction
The process of illuminating a hologram with a beam such that the hologram acts as a diffraction grating.

shape and structure. This information influences the choice of model. For objects such as colloidal particles, which might be described as spheres[19–21], ellipsoids[22], sphero-cylinders[23] or clusters of spheres[24], models can be based on exact solutions to Maxwell's equations that describe the scattering. For other specimens, such as living cells, either the scattering can be numerically simulated[23,25,26] or the specimen can be modelled as a simpler shape, such as a sphere. In each of these cases, the scattered field $\mathbf{E}_{scat}(\mathbf{r})$ is a function of the object's 3D position ($\mathbf{r}$), orientation, refractive index and size. We can predict the intensity $I(\mathbf{r})$ of the hologram by accounting for the interference with the reference field $\mathbf{E}_{inc}(\mathbf{r})$:

$$I(\mathbf{r}) = |\mathbf{E}_{inc}(\mathbf{r}) + \alpha\mathbf{E}_{scat}(\mathbf{r})|^2 \qquad (1)$$

where the phenomenological parameter α accounts for imperfections in the illumination[21].

Modelling enables three different approaches to hologram analysis. In the first, we directly fit the model to an experimentally captured hologram to infer information about the object — a generative modelling approach. In the second, we use modelling to train an algorithm to classify and quantify features from experimentally captured holograms — a machine-learning approach. In the third, we use machine learning to estimate parameters and then refine these estimates by fitting a generative model — a

Tomograms
Images recorded by a penetrating wave that represents a cross section of a 3D object.

Colloidal particles
Nanoparticles or microparticles suspended in a fluid or other medium.

Scattering
The interaction of electromagnetic radiation with an object resulting in a change in the direction of the light.

Coherent
Light that has a narrow distribution of frequencies and a well-defined phase, such that interference can be observed.

hybrid approach. As we shall show, a lot of information can be extracted from a hologram, including the object's size, orientation and composition, as well as its 3D location (FIG. 1b). The uncertainties in these measurements can be remarkably small. The size and 3D position of a microscopic object can be measured to nanometre-scale precision, whereas the refractive index and orientation can be measured to parts per thousand precision[21].

Where high-precision measurements are the main goal, a model-based analysis has several advantages over reconstruction. First, model-based analyses directly give values and uncertainties for quantities of interest. By contrast, reconstructions and tomograms are images — albeit 3D ones — that do not quantify the properties of the specimen without further analysis. Second, models account for the complex scattering of objects similar in size to the wavelength of light, such as colloidal particles or bacteria. For such objects, diffraction can distort reconstructions[27]. Third, model-based analyses yield precise results even with the simplest optical set-up, the in-line configuration shown in FIG. 1a. Unless otherwise stated, in this Primer we use the term holographic microscope to refer only to this microscope configuration.

The wealth and precision of information that can be extracted from in-line holograms with a model-based approach enable a host of applications, including 3D tracking of colloidal particles, measuring the forces exerted by cells, analysing the composition of complex dispersions and performing sensitive biochemical assays (FIG. 1c). Many of these applications benefit from the speed of a holographic microscope. Holograms can be collected as quickly as the camera records images because no mechanical adjustments are needed to keep the object in focus; any movement in the axial direction can be measured from the fringes. Typically, analysing holograms takes more time than acquiring them. However, many sensitive and sophisticated analyses can be done in near real time on a personal computer.

The model-based approach requires a careful choice of analytical method and some prior knowledge of the sample. As a result, it has some limitations, which we discuss in the penultimate section of the Primer. Other sections explore how to create and use a holographic microscope, how to analyse the data, what measurements can be made, and what reproducibility issues might be encountered and how to overcome them. In the final section we consider the future of model-based analysis, an emerging paradigm for microscopy.

Experimentation

Instrument layout. One can convert an optical microscope into an in-line holographic microscope by making the illumination coherent, as shown in FIG. 2a. The new illumination source can be either a laser or a
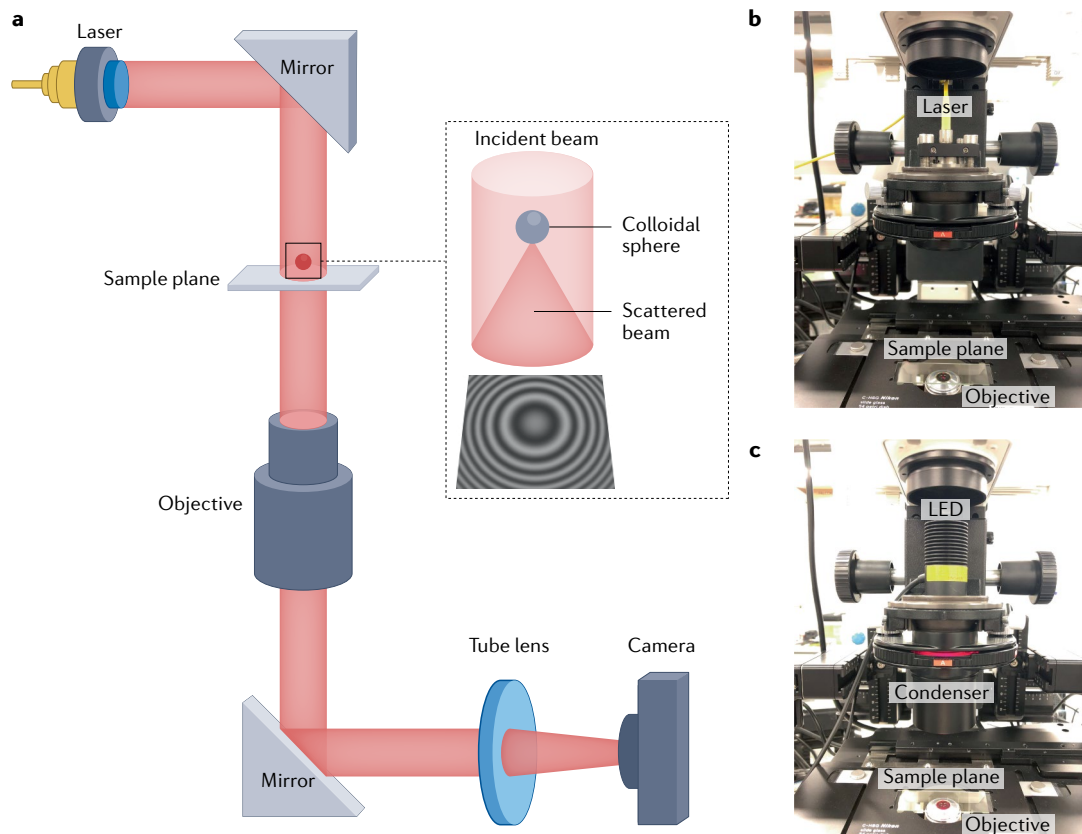

Fig. 2 | **Detailed set-up of an in-line holographic microscope. a** | Beam path and optical layout for an in-line holographic microscope with coherent illumination. A single-mode fibre coupled to the laser spatially filters the beam. The filtered beam (red) is steered to the sample plane, where it scatters from the specimen. The scattered and transmitted beams go through the objective and tube lens to the detector. **b** | Photograph of an in-line holographic microscope with a fibre-collimated laser source and no condenser lens, built on a standard inverted optical microscope. **c** | Photograph of an in-line microscope with a light-emitting diode (LED) source, where the inbuilt condenser lens collimates the partially coherent source.

partially coherent source, such as a single-colour light-emitting diode (LED). The illumination beam should be collimated and directed into the sample. Light passing through the sample is collected by the microscope's objective lens and projected by its tube lens onto an area sensor, typically a complementary metal oxide semiconductor camera. If the sample is not too dense or opaque — the usual condition under which optical microscopy is performed — the incident beam will be weakly scattered, such that most of it is unperturbed. This unperturbed, transmitted light then interferes with the light scattered by the sample to form a hologram.

To integrate a coherent illumination source with the microscope, we place a fibre-collimated laser with narrow spectral bandwidth[28] between the illuminator and the phase ring turret/condenser, as shown in FIG. 2b. We use single longitudinal-mode diode lasers because they are inexpensive and bright. Furthermore, their coherence length is not too large, so that reflections from various glass surfaces in the microscope do not produce extraneous interference in the hologram. Alternatively, one can use a partially coherent source, such as an LED, as shown in FIG. 2c. The low temporal and spatial coherence of LEDs can further suppress extraneous fringes and speckle relative to a diode laser[29]. The longitudinal coherence length of commercially available LED sources is in the order of a few micrometres, which is large enough to obtain holograms of objects smaller than this scale, such as colloidal particles. Inserting a pinhole between the LED and the sample increases the spatial coherence but also reduces brightness[30,31]. One must collimate the LED source by adjusting the distance between the LED and the microscope's inbuilt condenser lens. If the illumination source is already collimated, the condenser can be removed from the beam path.

Model-based analysis of holograms is most effective if the incident mode has the simplest possible structure. Therefore, we spatially filter the illumination source by, for example, coupling the laser source to a single-mode fibre. The illumination beam can then be reasonably described as a plane wave. We set or measure its polarization, which we need to model the scattered field.

The choice of objective lens depends on the size of the object to be imaged. For micrometre-scale objects, we use an objective with a high numerical aperture, such as an oil-immersion or water-immersion lens. Although a water-immersion objective has a lower numerical aperture than an oil-immersion objective, it is potentially more useful for aqueous specimens because it reduces the spherical aberration introduced by a glass coverslip[32]. In either case, it is important to select an objective that does not contain a phase plate, an inbuilt optical element used for phase-contrast microscopy, which would distort a hologram.

It is also possible to eliminate the objective lens altogether. One can construct a lensless holographic microscope from a coherent light source, a pinhole and a sensor placed close to the sample[30,33]. Lensless microscopes tend to have a small effective numerical aperture and a large effective pixel size. They therefore cannot collect the strongly diverging light scattered by small particles or resolve finely spaced interference fringes. Lensless

holography therefore is most effective for tracking and characterizing particles that are several times larger than the wavelength of light.

Sample preparation. Scattering from the sample chamber can add unwanted background interference to a hologram. To minimize background interference, we place our specimens in a sealed sample cell consisting of two glass coverslips separated by a spacer about 100 μm in height. The spacers can be silicone-based vacuum grease, double-sided tape, thin strips of plastic affixed with UV-curable epoxy or silicone gaskets. We avoid evaporation and undesired flow by sealing the chamber with silicone grease or epoxy.

Some experiments require the sample to flow through the microscope's observation volume. To make a simple flow chamber, we place spacers between two glass surfaces and leave the edges unsealed. We then add a droplet or an absorbent material to one end to draw fluid through the channel by capillary action. To drive flow in more sophisticated flow chambers, such as microfluidic chips[34], we use syringe pumps or pressure pumps. We reduce interference due to reflections by making the channels wider, imaging the objects or particles only when they are a few micrometres away from the walls or matching the refractive index of the fluid medium to that of the wall material. Flow enables high-throughput experiments, but one can also use an automated stage and a multi-well sample plate to carry out such experiments without flow.

Interfaces between fluids with different refractive indexes can significantly distort holograms. Holograms of particles at or near an interface should therefore be made in regions where the interface is flat. To encourage an air–water or oil–water interface to remain flat, we pin the interface[35] using a machined or 3D-printed chamber with a thin, flat lip.

Holograms can also be degraded by non-uniform illumination[36], by undesired scattering from dust particles or other out-of-focus objects and by optical aberrations[37]. If the hologram formation model does not correct or account for these effects, they can introduce errors into the inferred information. A spatial filter can alleviate non-uniform illumination, whereas a low-coherence source, such as a laser diode or LED, can attenuate holograms from out-of-focus objects. Cleaning the coverslips — by, for example, plasma cleaning, rinsing with purified water and drying with nitrogen — reduces background scattering from dust in or on the sample chamber. If the sample solution is sufficiently dilute, the hologram of the object of interest will not substantially overlap with holograms of other objects. Typically, the sample should be dilute enough for the particles or objects to be at least a few micrometres apart[38]. With a dilute system, one can also record images with no objects in the field of view and use these images to correct for background scattering. Finally, a water-immersion lens can minimize the effects of spherical aberration. Alternatively, spherical aberration can be incorporated in the model[37].

Data collection. The camera on a holographic microscope does not need to be expensive. For experiments involving a single illumination source, we use a monochrome
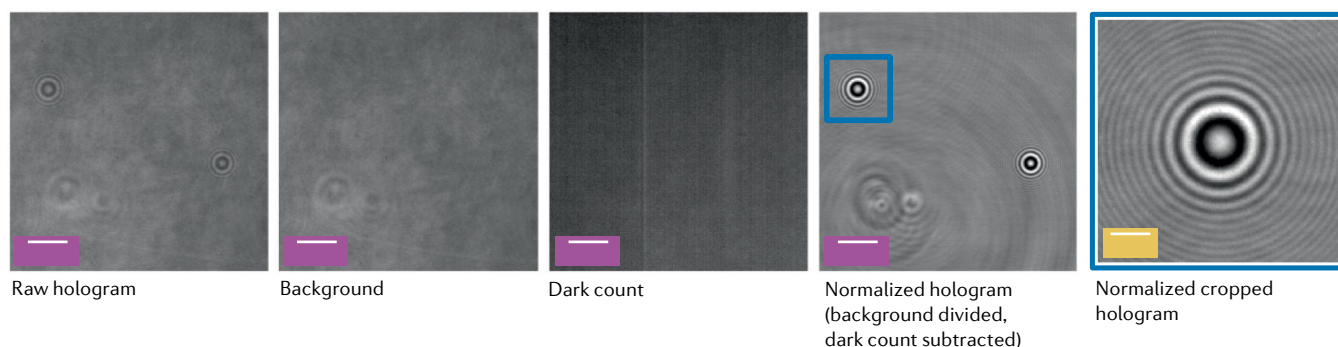
Fig. 3 | **Data normalization for hologram analysis.** To normalize a hologram, we subtract a frame-averaged dark count (middle) from a raw hologram (far left) and then divide by a dark count-corrected background image (second from left). We then crop the normalized hologram (second from right) around the feature of interest associated with a particle (far right). The extent of the cropped hologram depends on the size of the specimen and its distance from the focal plane. Purple scale bars = 15 μm; yellow scale bar = 5 μm.

sensor, because the filters on a colour sensor reduce sensitivity and spatial resolution. Shortening the exposure time reduces motion blurring[39,40] at the expense of the overall image intensity. Increasing the illumination intensity can compensate for this effect. The quality of the recorded image is limited by the signal-to-background ratio, which favours photodetectors with a dynamic range large enough to capture bright fringes without saturation and dark fringes without underexposure. High quantum efficiency is not necessary and can be counterproductive, as the reference wave produces a large background signal that can saturate a high-efficiency detector. Therefore, the cooled, high quantum efficiency, expensive cameras used in single-molecule and other precision microscopy techniques are unsuited to holographic microscopy.

Fast cameras enable experiments on fast-moving or quickly changing specimens. They require hardware that can handle their high data rates. For example, a 1-megapixel camera operating at 1,000 frames/s transfers 1 GiB/s of 8-bit greyscale images to a computer. This computer needs a fast interface — the latest USB, 10-Gb ethernet or a proprietary connection, often operating on a dedicated controller card — a fast internal bus to transfer the data and a solid-state drive with a high write speed. We recommend a computer with the latest peripheral component interconnect express (PCIe) bus for rapid, parallel data transfer and, ideally, a large amount of random access memory (RAM) to buffer the data stream. Many cameras come with their own proprietary control software, but the academic community has also developed open-source software such as μManager[41], which can be used to control various models of camera and the microscope itself.

Some processes, such as cells flowing through a channel at high speed[42], may be so fast that features of interest are blurred even at the shortest camera exposure times. For such processes, we pulse a laser diode to illuminate the samples for a short time (microseconds), as in strobe photography. Many cameras include synchronization input and/or output ports. We use these ports to synchronize the camera and laser diode with each other or with a pulse generator[43,44].

Results

Holograms encode comprehensive information about the position and composition of individual particles or biological specimens. In a model-based analysis, we extract this information by fitting a generative model to the hologram[20,21,23,45–47], by analysing the hologram with a trained machine-learning system[48–50] or by some combination of the two. Although all three approaches require minimal processing of the hologram, some pre-processing is beneficial for reliable results. We typically normalize holograms by subtracting the dark count from both the raw hologram and background and then taking their ratio[51], as shown in FIG. 3. These linear transformations remove instrument-dependent effects and facilitate comparison with models. We obtain dark counts by recording images with the illumination off, and we obtain background images by recording fields of view with no particles in frame, ideally at the same axial position as the data.

After normalization, we crop the hologram to the region of interest, which is typically a few hundred pixels wide. The size of the cropped hologram should be large enough to capture many hologram fringes, but small enough to avoid overlap with nearby objects. We automate this process by using algorithms based on Hough transforms[39,52,53] or machine learning[49,50].

The computational power required to extract information about the specimen depends on the number of pixels in the hologram. However, the fringes of a hologram are often symmetric, and therefore much of the information is redundant. Consequently, most of these pixels can be discarded. Dimiduk and Manoharan found that by randomly selecting[54] just 2.5% of pixels and discarding the rest, they could accurately analyse holograms while reducing the computational time by an order of magnitude[55]. Selecting a random subset of pixels is now a standard part of our hologram pre-processing routine.

Generative modelling. To explain the generative modelling approach, we first consider inferring physical information about a single spherical particle from its hologram, as shown in FIG. 4. A generative or forward model can realistically simulate the hologram of such

Dynamic range
The range of intensities that a sensor can record.

Quantum efficiency
A measure of the sensitivity of a detector, determined by how many incident photons are converted into electrons.

Dark count
The intensity recorded by a sensor or camera in the absence of a signal.

a particle as a function of its position, size and optical properties. One can then fit the model to the data to infer these parameters. The simplest fitting approach is to iteratively modify the parameters until the differences between the model and data are minimized.

A generative model of a single spherical object might use Lorenz–Mie theory[19] — the exact solution to Maxwell's equations for scattering from a spherical particle — to calculate the scattered field. It would then simulate a hologram by calculating the interference between this field and a planar reference wave[20,21]. Such a model includes six parameters: the size and refractive index of the sphere, its 3D position and α, the phenomenological parameter from Eq. 1. The hologram recorded on the detector is treated as a magnified image of the hologram at the objective's focal plane.
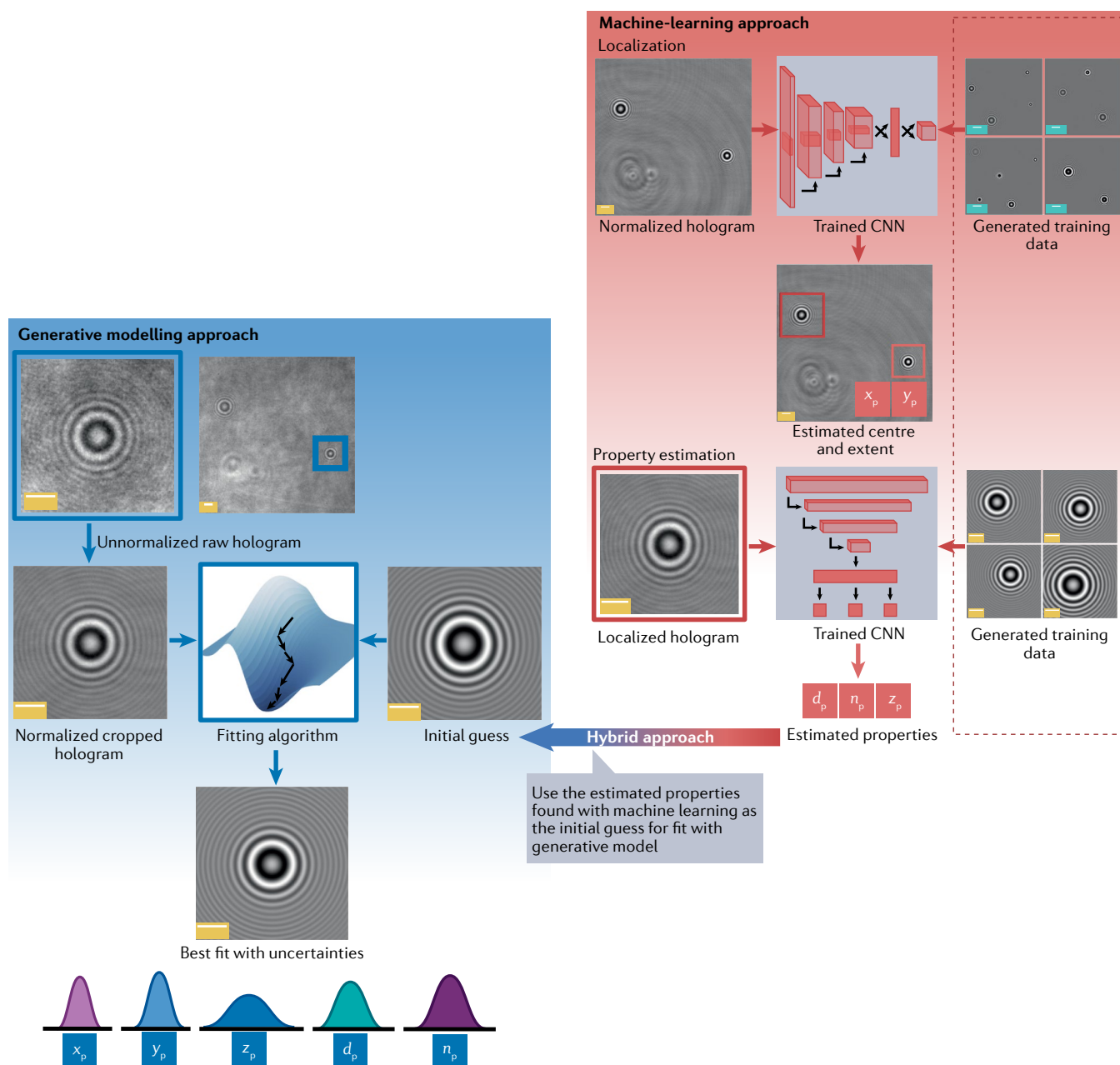

Fig. 4 | **Approaches to quantitative analysis of holograms.** Flow chart of approaches to hologram analysis, in which a single colloidal sphere serves as an example specimen. In a machine-learning approach, neural networks trained with generated data detect, localize and estimate the properties of particles. In the localization module, an object-detection convolutional neural network (CNN) detects any holographic features in a normalized field of view and determines the centre, x_p and y_p, and extent of each detected feature. A property estimation module, which is also a CNN, estimates the particle's diameter d_p, refractive index n_p and axial position z_p from the cropped holograms. In a generative modelling approach, the first steps are normalizing and cropping the field of view around the hologram of interest, which is automatically detected with a Hough transform. A non-linear least-squares or Markov-chain Monte Carlo algorithm then fits a generative model of hologram formation to this cropped hologram. A non-linear least-squares fit requires an initial guess, which can be informed by experimental expectations, and returns the best-fit parameters and their uncertainties. In the hybrid approach, a machine-learning module first estimates the parameters, and a fitting module then refines these estimates using the parameters from the machine-learning module as the initial guess to the fit. Turquoise scale bars = 10 μm; yellow scale bars = 5 μm.

To fit this model to a recorded hologram, one can use a non-linear least-squares method such as the Levenberg–Marquardt algorithm[56]. If the fitting algorithm is given a good initial guess, it can find parameter values that globally minimize the discrepancy between the model and the recorded hologram. Fitting the single-sphere model to data yields precise estimates of the sizes, optical properties and 3D positions of individual colloidal particles[21]. This approach has been applied to measuring diffusion[57,58], quantifying interactions between a sphere and fluid interface[35,59,60], tracking particle motion in an optical trap[61–63], differentiating species of particles within a mixture[49,64–66], measuring the growth of colloidal particles during chemical synthesis[67] and inferring the refractive index[68] and rheological properties[69] of the medium in which the spherical particles are embedded.

Perhaps more surprisingly, the single-sphere model is a useful approximation for non-spherical objects such as dimpled spheres[51], protein aggregates[66,70], colloidal aggregates[71,72] and dimers of colloidal spheres[73]. The advantage of using a single-sphere approximation to model these systems, compared with a more realistic model, is that the single-sphere model can be fit more rapidly to the data. The speed of fitting makes it particularly useful for high-throughput applications, such as industrial quality assessment and process control[70], wastewater treatment[74] and slurry analysis[66,75], in which particle size and composition must be determined continuously in real time.

Where analysis speed is not the primary concern, Bayesian parameter estimation can yield more detailed information on uncertainty and can more easily incorporate prior information than non-linear least-squares fitting. A non-linear least-squares fit yields a single set of parameters that best fits the data, whereas a Bayesian analysis yields the posterior probability density (posterior) of all possible combinations of parameters. Peaks in the posterior correspond to sets of parameters that fit the data well and are not excluded by any prior information. The prior information might include a previous calibration of the particle size distribution or the anticipated refractive index of the material. The width of a peak in the posterior characterizes the uncertainty of the parameter estimates.

The Bayesian approach can also determine marginalized uncertainties (FIG. 4), which account for correlations between parameter estimates[55]. For example, the best-fit particle size is typically correlated to the axial position, as both affect the fringe spacing. If one cares only about the particle size, one can marginalize — or integrate out — the axial position, effectively incorporating its correlations into the uncertainty of the size estimate. Marginalization yields realistic uncertainties. It is particularly useful for fundamental studies that test theories of dynamics or interactions, and for applications that have specified tolerances — for example, on particle size.

More complex generative models can be used for non-spherical specimens. Exact solutions to Maxwell's equations exist for spheroids, ellipsoids, sphero-cylinders, coated spheres and small collections of spheres[76]. There are also numerical models for these

shapes and for many others, including those with no exact solutions[23]. Generative models for these specimens, such as models for single spheres, calculate the scattered field and simulate its interference with a planar reference wave. But models of non-spherical specimens have additional parameters such as shape, orientation or multiple refractive indices and radii. Consequently, it takes more time to fit such models to the data.

Generative models can also account for the effects of the microscope's optical train. The single-sphere model approximates the scattered field poorly when the particle is close to or below the focal plane. The inaccuracies of the model therefore limit the depth of field available for particle tracking. To circumvent this problem, Leahy et al. modelled the effects of an objective lens on the hologram of a spherical particle and then fit this model to data. They found that for a 2.4-μm sphere imaged with a water-immersion lens, the region of accurate tracking increased by a factor of two relative to a lens-free model[77]. Martin et al. showed that extending this model to incorporate the effects of spherical aberration, a common aberration in optical microscopy, increases the accuracy of particle characterization[37]. These lens models work with scattering models for either spherical or non-spherical objects. For non-spherical objects, they are slow because they must numerically integrate the scattered field to calculate the effect of the objective[78]. For spheres, they are quick because the integral can be analytically simplified.

A Bayesian approach is useful for more complex models because it can account for the many ways a model might fit the data. Consider a capsule-shaped bacterium that has a small shape asymmetry between its head and tail. Even if the generative model includes this asymmetry, fitting might not unequivocally determine the bacterium's orientation from the hologram. In the presence of noise, both orientations might fit the data equally well. In this case, the posterior would show two modes, one for each orientation, accurately reflecting the uncertainty in the measurement. This uncertainty can then be propagated to other quantities. If prior information excludes one orientation — for example, if the bacterium is swimming in a known direction — this information would be reflected in the posterior, which would have a single peak.

For the Bayesian approach, we use Markov-chain Monte Carlo (MCMC) methods[79] to calculate the posterior probability and to obtain marginalized uncertainties. Some MCMC methods require a good initial guess, which can be obtained using algorithms such as covariance matrix adaptation evolution[80]. Other methods, such as Hamiltonian Monte Carlo[81] and parallel tempered MCMC sampling[82], do not require a good initial guess. We use these methods to efficiently explore the high-dimensional parameter spaces of complex models.

The choice of generative model depends on the experimental aims. When the aim is to track a spherical object in three dimensions, we recommend a generative model that includes lens effects. With such a model, one can fit holograms above and below the microscope focal plane. When the aim is to characterize the properties of spherical objects, we recommend using a generative model

Bayesian parameter estimation
A statistical inference technique yielding the probability distribution of the parameters of a model given the data.

Marginalized uncertainties
The uncertainties in a model parameter determined by accounting for correlations with other parameters.

Markov-chain Monte Carlo
(MCMC). A numerical method that uses a biased random walk through the parameter space to both estimate a probability distribution and integrate it.

that accounts for spherical aberration. Such a model enables more accurate quantification. When the aim is high-throughput characterization, we recommend using a single-sphere approximation, which allows real-time analysis. One rarely has to write the generative model from scratch. Open-source packages such as HoloPy[83] and pylorenzmie include generative models for different types of particles and lens effects. They also include non-linear least-squares and MCMC methods to fit these models to data. Tutorials are available for HoloPy and pylorenzmie.

Machine-learning analysis. Machine learning offers alternatives to conventional algorithms for feature identification[84,85], particle tracking[86] and quantitative hologram analysis[13,20,21]. As with the generative modelling approach, the aim is to determine an object's position and properties directly from its hologram. But instead of modelling the physics of image formation, convolutional neural networks (CNNs) or support vector machines recognize, classify or characterize objects based on training data. In general, machine-learning approaches work well on problems with many degrees of freedom; they recover low-dimensional solutions that classify or characterize the data[87]. For holography in particular, machine-learning approaches are well suited to problems where generative modelling is computationally expensive, such as characterizing particles in a high-throughput experiment.

We use machine-learning approaches to tackle three types of analysis problems in holography: localization — estimating the hologram's centre and extent in the field of view[49,50,88]; property estimation — characterizing the object's refractive index, diameter and axial position[48,89]; and classification — differentiating and labelling the structure of the particle[90]. Combining the modules used for each of these analysis steps results in a full end to end analytical pipeline for holograms[50].

Each of these three tasks requires training a model. Training consists of feeding holographic image data with known parameters — such as known particle size and position — to the model, which learns to recognize patterns in the data and the parameters. In many machine-learning applications, one must gather and manually annotate training data. The cost of human labour in this process limits how much training data can be produced, and thus reduces the model's accuracy. The application to holographic microscopy has an advantage because the generative models can rapidly generate large amounts of properly annotated training data.

The amount of training data needed for an analysis task depends on the size of the parameter space and the desired precision of the classification. For the training data to span the range of interest $R(p_j)$, where p_j is one parameter in a set of M coupled parameters and Δp_j is the desired resolution of that parameter, the number of training elements must scale as $N \leq \prod_{j=1}^{M} R(p_j)/\Delta p_j$, where the upper limit corresponds to calculating every possible solution. For non-spherical objects, the training data must span all possible orientations, positions, sizes and refractive indices. Sampling approaches can reduce the number of elements below the upper bound.

To better match experimental conditions, one can intentionally degrade the simulated holograms with either uniform Gaussian noise[50] or noise directly extracted from the experimental holograms, including both camera noise and time-varying fluctuations[90]. Adding noise prevents the model from overfitting experimental data, thereby improving the accuracy of the results[50,90].

Training involves optimizing the parameters of the model to accurately fit the labelled training data. Various optimizers are available, including Adam[91], root mean square propagation and stochastic gradient descent[92]. Activation units such as ReLU enable the model to learn complicated functions and facilitate rapid training[93]. In our experience, the training speed is limited by how quickly training data can be generated, although that process can easily be parallelized and is a one-time cost. With current computing clusters, we can generate data and train a model in a few hours[90].

The first step in hologram analysis is localization, which involves finding the regions of interest in a hologram that correspond to particular objects, as shown in FIG. 4. CNNs are particularly well suited for object detection and localization[48,50,94]. We first train the CNN on synthetic holograms with variable numbers of particles. The CNN then takes a greyscale image input and returns a set of cropped images centred on each particle, along with the estimated parameters of the hologram centre, x_p and y_p, and the extent of each detected feature. We can then use the number of identified features to measure particle concentrations or pass each cropped hologram to another module for further analysis.

Machine-learning algorithms are both more accurate and more robust than conventional object detection algorithms[39,85], yielding much lower rates of false positive and false negative detections. The localization algorithm used by Altman and Grier[50], for example, missed fewer than 0.1% of simulated holograms across a wide range of particle sizes, refractive indexes and positions. By contrast, conventional algorithms missed up to 40%. This ability to detect particles over wide regions of the parameter space is necessary for robust, unattended particle tracking and characterization.

After localizing and cropping the hologram, we use other machine-learning systems, such as CNNs[50,89] or support vector machines[48], to estimate the properties of the objects. First, we scale the block of pixels identified in the localization stage down to a standard size, which enables the algorithm to accommodate holograms with different extents in the camera plane. The network then reduces the dimensionality of the data until it outputs values for the particle properties, including diameter d_p, refractive index n_p and axial position z_p.

Although the generative modelling approach yields more precise and accurate property estimates, machine learning is faster and more flexible[50]. End to end processing of a full-frame hologram takes 30 ms or less[50]. In addition, machine-learning models require little tuning or prior knowledge of the system, and they are more resilient to artefacts that can hinder the performance of generative models[50].

Machine-learning methods can also classify the structure of a specimen. For example, CNNs can recognize

Convolutional neural networks
(CNNs). Machine-learning algorithms that use convolution layers to process higher-dimensional image data.

Support vector machines
Machine-learning algorithms that distinguish data points using hyperplanes in a high-dimensional parameter space.

ReLU
The rectified linear activation function, a piecewise function that returns zero for negative inputs and returns the input for positive inputs.

and differentiate clusters of colloidal particles bound by short-range attractions[95]. Because the range of the attraction in such clusters is only about 10% of the particle diameter, standard optical microscopy techniques cannot easily distinguish bound and unbound particle pairs. Furthermore, the computational cost of fitting a model to the hologram is high. Klein[90] instead detected differences in cluster configurations using a standard, pre-trained CNN image classifier[96] that was re-trained with simulated holograms augmented with experimentally extracted noise. The re-trained CNN extracted hierarchical features from the hologram and classified them to determine the configuration of particles. Klein found that after including experimentally extracted noise in the training data, the re-trained CNN could differentiate six different ground states of a seven-particle cluster — including two states differing by only one pair of bound particles — with 60–80% accuracy.

Free, open-source software[50] — Characterizing and Tracking Colloids Holographically (CATCH) — is available for end to end analysis of holograms from spheres and other particles that can be usefully modelled as spheres. A tutorial (CATCH) is available. For other applications, models must be built and trained. However, the architecture of the neural network does not need to be rebuilt for each problem; instead, existing machine-learning frameworks for image analysis can be used[90].

Hybrid approaches. Current machine-learning methods for analysing holograms are fast and robust, but not as precise or accurate as generative modelling approaches. Conversely, generative modelling approaches are highly precise and accurate, but incur higher computational costs than machine-learning methods. A hybrid approach offers the best of both worlds: fast, automated analysis with high precision.

A hybrid analysis pipeline begins with a machine-learning stage. From a full-frame hologram, a trained network automatically localizes and crops holograms corresponding to individual objects. It then estimates their properties, which might include their refractive indices, diameters and axial positions. In a second stage, an algorithm fits a generative model to each cropped hologram, using the machine-learning estimates as initial guesses.

Machine learning eliminates the need for human input to the fitting routine. The algorithm determines the number of objects in the field of view, the extents of their holograms and the initial guesses required to fit the model to the data. This hybrid approach also enables fully parallel analysis of time-series data. In a generative modelling approach, one usually derives initial guesses for each frame in a time series from the best-fit parameters of the previous frame. Consequently, the frames must be analysed sequentially. But the machine-learning approach provides initial guesses for all frames, which one can use to fit generative models to all frames in parallel.

In principle, machine-learning approaches could also select the appropriate generative model by classifying the structure and shape of the specimen. Such an approach could automate the entire hologram analysis pipeline.

Applications

The direct analysis of holograms has enabled new, high-precision measurements of colloids, soft materials and biological systems. In this section, we highlight a few examples.

Colloidal dynamics and self-assembly. The precision enabled by the generative modelling approach was crucial to discovering an unexpected feature of colloidal systems. Since the early twentieth century, it was known that micrometre-sized solid particles could stick irreversibly to the interface between two fluids[97]. This phenomenon, driven by surface tension, is the basis for making the solid-stabilized Pickering emulsions now used in foods[98], oil recovery[99] and many other applications[100,101]. The interface can also serve as a scaffold that guides the self-assembly of these colloidal particles[102]. Until recently, it was assumed that the particles would approach the interface, breach it and then immediately reach an equilibrium position, as shown in FIG. 5a.

Holographic microscopy showed that, contrary to initial assumptions, the particles take a long time to relax to equilibrium after they breach the interface. Kaz, McGorty et al.[35] used radiation pressure to push a particle upwards to a planar oil–water interface while measuring its height using a holographic microscope. By fitting a single-sphere generative model to the holograms, they were able to measure the height to nanometre-scale precision on millisecond timescales (FIG. 5a). With this combination of high spatial precision and high temporal resolution, they observed the motion of the particle immediately after the breach and showed that it scales logarithmically with time (FIG. 5a). The long duration of the measurement allowed them to observe this scaling over multiple decades and enabled comparison with theory. The logarithmic behaviour is a signature of pinning and depinning of the three-phase contact line on the particle, which leads to surprisingly long relaxation times — of the order of months for a micrometre-scale particle.

Later holographic microscopy experiments showed that this long-time relaxation is common to many different types of colloidal particles[59,60,103]. Wang et al.[22] showed that when ellipsoids breach an interface, the particles rotate far more slowly to equilibrium than previously predicted. They revealed this motion by fitting a generative model for scattering from an ellipsoidal particle as a function of orientation and position. These studies illustrate how the generative modelling approach leverages the strengths of holographic microscopy: its acquisition speed, high dynamic range and sensitivity to the 3D position and orientation of the particle.

Holographic microscopy is also well suited to answer questions about how colloidal particles interact and diffuse. The structure and dynamics of these systems are difficult to determine with standard optical microscopy because the interactions are so short ranged — a few tens of nanometres — and because the particles diffuse in three dimensions. Using holographic microscopy, Fung and co-workers imaged the 3D motion of pairs of interacting colloidal particles with high temporal resolution. They resolved the translational, rotational and

vibrational motion of the particles — and their interaction potential — by fitting generative models that account for scattering from multiple spherical particles, including near-field and far-field couplings between the scattered fields[24,104]. Perry et al.[105] used a similar approach to infer the 3D dynamics of self-assembled colloidal clusters as they transitioned between free-energy minima (FIG. 5b). The structure and dynamics of these systems can give insights into the first stages of crystal growth and the mechanisms of self-assembly in colloidal systems. The precision of this measurement was sufficient to resolve transitions between two free-energy minima for a six-particle cluster, which was not possible with wide-field or confocal optical microscopy.

Microrheology and stress measurements. Measurements of colloidal dynamics not only can reveal information about the physics of interacting systems but can also reveal information about materials in which colloidal particles are embedded. In microrheology, for example, one infers the viscoelastic properties of a material by measuring the Brownian motion of embedded tracer particles[106]. In traction-force microscopy, one infers the forces exerted by living cells by measuring the motion of particles embedded in an elastic substrate that deforms as the cells move on it[107]. In both cases, one needs to detect small displacements of the particles. Typically, a confocal or a standard wide-field optical microscope is used, but a holographic microscope has advantages.
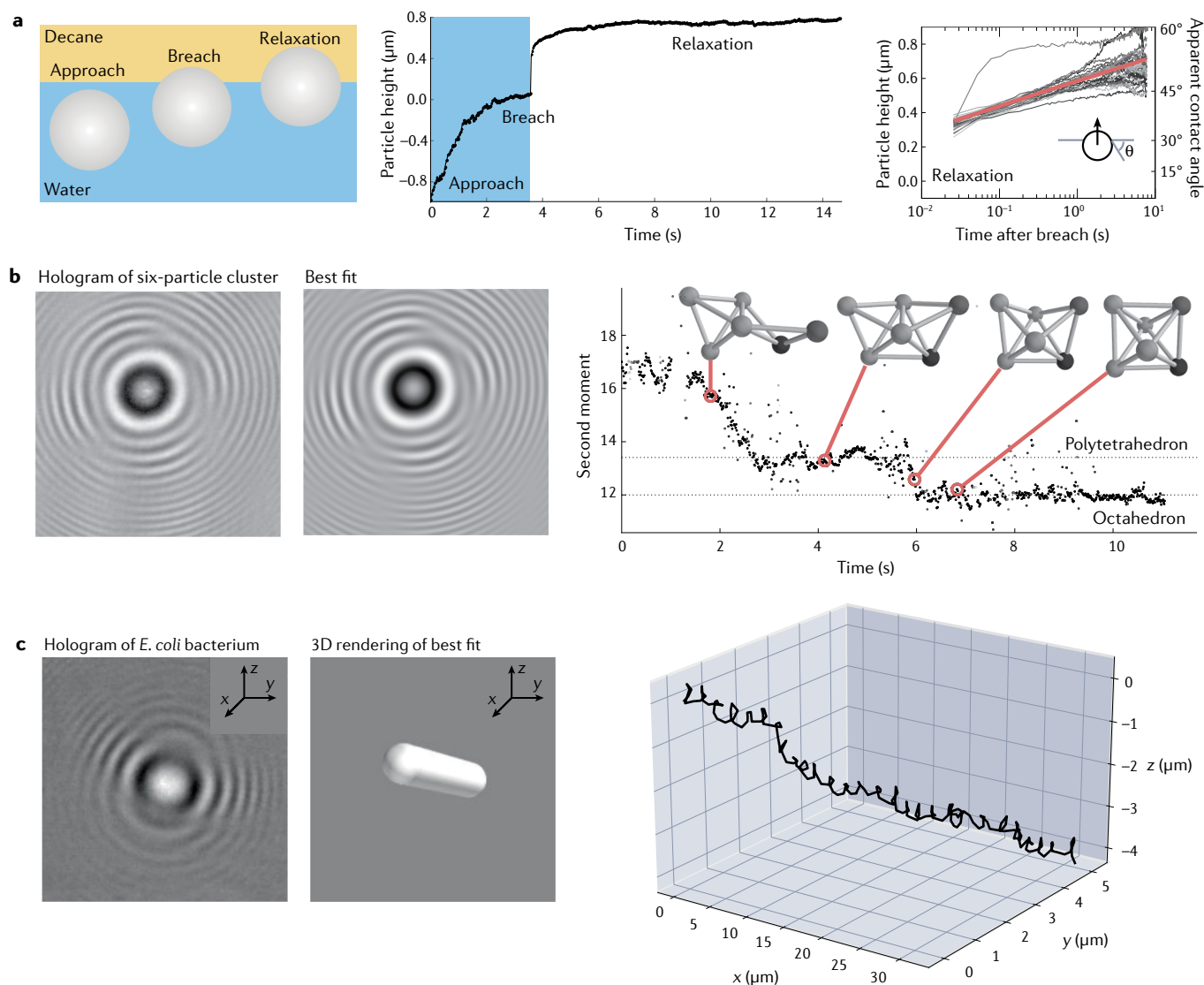

Fig. 5 | **Motion and tracking. a** | A colloidal particle approaching and breaching an interface between two fluids (left). Plot showing the position of a particle before and after the breach (middle). The high-precision tracking of holographic microscopy shows that the particles relax logarithmically in time to equilibrium (right). Each curve corresponds to a measurement of a single particle. **b** | Fitting a generative model to holograms of a six-particle cluster of interacting spherical particles reveals transitions between states. The raw hologram is shown alongside the best-fit hologram (left). The results of the fits quantify the evolution of the cluster structure, represented by the second moment of the mass distribution. The full structures are shown as ball-and-stick models for four time points highlighted in red. **c** | Hologram of a single *Escherichia coli* bacterium (left) shows asymmetry in the fringes. Fitting a generative model of a sphero-cylinder (middle) to this hologram yields estimates of the orientation and position of the bacterium as it swims. The high positional and angular precision reveal a helical wobble, clearly distinct from Brownian motion, in the swimming pattern, shown in the 3D plot (right). Part **a** adapted from REF.[35], Springer Nature Limited. Part **b** adapted with permission from REF.[105], RSC. Part **c** adapted with permission from REF.[114], Optica Publishing Group.

Microrheological measurements benefit from the higher precision of the holographic microscope. Modelling and fitting a time series of holograms reveals the motion of tracer particles with nanometre-scale precision. The diffusion coefficient[24,104,108] of the particles and the viscoelastic properties of the medium can then be inferred from these 3D motion data. Cheong et al.[69] used this approach to precisely measure the complex viscoelastic moduli of polysaccharide gels, obtaining accurate measurements in micrometre-scale samples without mechanical loading.

Traction-force measurements benefit from the depth of field of the holographic microscope. Makarchuk et al.[109] obtained the full 3D displacement map of tracer particles without scanning the focus of the microscope. They also measured the displacements to nanometre-scale precision. Although their technique did not use a generative model, it did involve directly analysing the hologram fringes to measure the forces exerted by colorectal cancer cells. The application of holography to traction-force microscopy could enable both higher time resolution and characterization of forces on stiffer substrates, where the embedded particle motion is subtler.

Microorganisms and organelles. Holographic microscopy can also measure the properties and motion of biological systems. Fluorescence microscopy is commonly used for such systems because fluorescent labelling offers excellent contrast for the object of interest. But labels can also interfere with biological systems. Furthermore, photobleaching limits the number of detected photons and, hence, the duration of experiments[110]. Because holographic microscopy is based on scattering, the number of photons that can be detected is unlimited. Instead, the precision and speed are limited by the scattering strength of the sample. Biological systems tend to scatter weakly because their refractive indices are usually close to the index of water (1.33). The refractive indices of living cells, for instance, are around 1.38 or smaller[111,112].

However, even weakly scattering microorganisms such as *Escherichia coli* can be seen under the holographic microscope. The small scattering cross section of an individual *E. coli* bacterium — which is about 2 μm long and has a refractive index of 1.388 (REF.[113]) — makes it difficult to see in a bright-field optical microscope. Wang et al.[114] were able to use holographic microscopy to capture the 3D swimming motion of these bacteria, including its tumbling, as shown in FIG. 5c. To obtain this information, they first modelled a bacterium as a homogeneous sphero-cylinder. They then fit a generative model of scattering from a sphero-cylinder to the data. This technique allowed them to measure both the position and the orientation of individual bacteria as a function of time. Using the high acquisition speed of the microscope, they resolved even the wobble of the bacterium during its run and tumble motion, as shown in FIG. 5c.

Holographic microscopes can also image vesicles, another class of weakly scattering systems that are biologically important. Vesicles are enclosed lipid bilayers that serve as models for organelles. They are used to deliver drugs[115], study the origins of life[116] or create artificial cells[117,118]. In these applications, the solute loading of the vesicle and its motion must be tracked over time. This is a non-trivial task because the bilayer is thin (about 5 nm). Consequently, the vesicle has a small scattering cross section[119]. But when the vesicle is filled with, for example, a sugar solution, its scattering cross section increases, and interference fringes become visible under the holographic microscope, as shown in FIG. 6a. One can fit a generative model for a core–shell spherical particle to holograms of such filled vesicles — where the core is the filling solution and the shell is the thin outer layer of lipids. The fit reveals the vesicle's refractive index and size, which can be used to quantify vesicle loading[120].
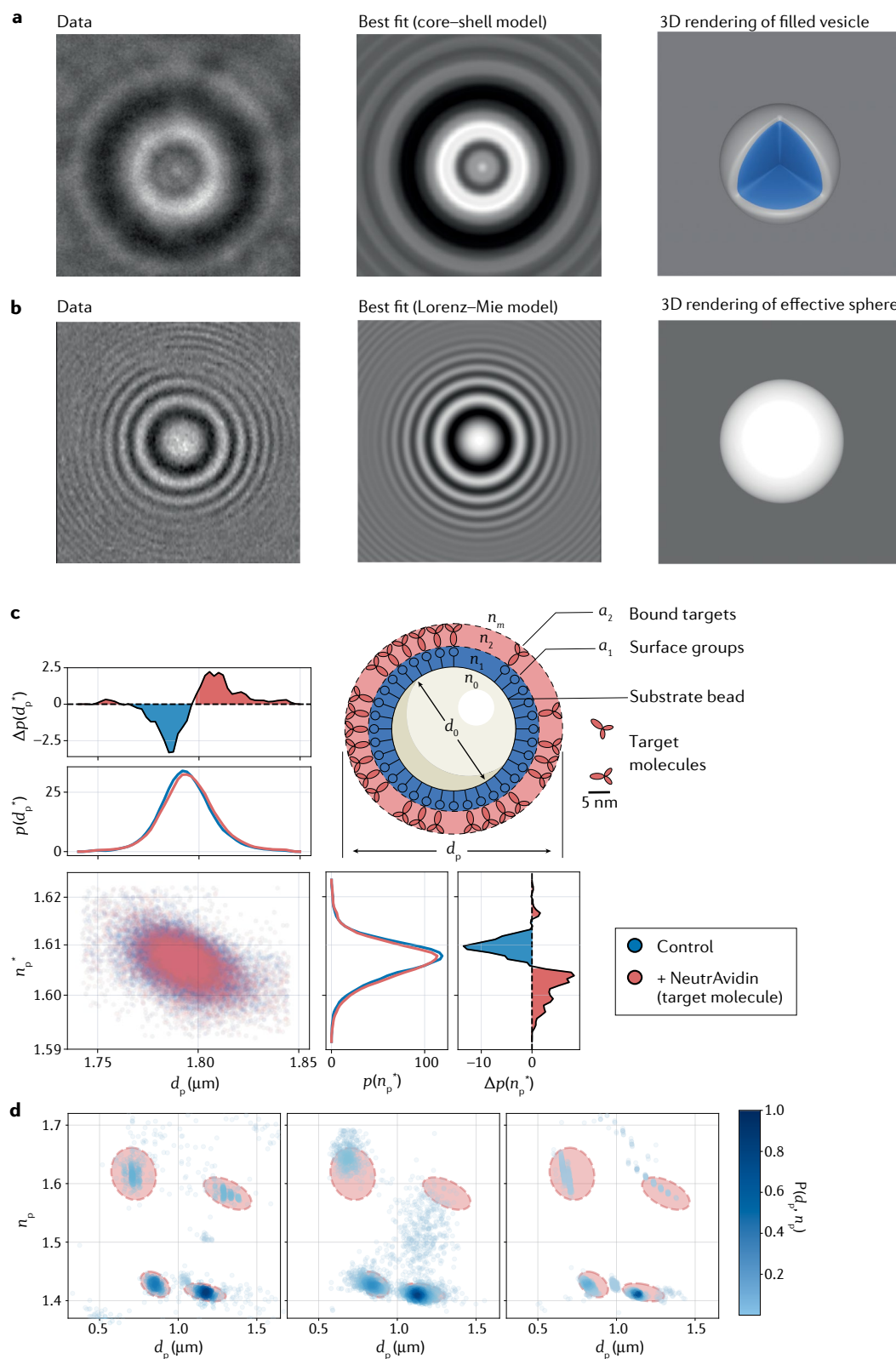
Detection of molecules. Macromolecules, such as enzymes or proteins, are too small to see with a typical optical microscope because they do not scatter enough light. One can detect them by fluorescently labelling them and measuring their fluorescence when they bind to a functionalized bead. As in other fluorescent measurements, labelling adds a step to the detection process, and labels can interfere with binding[121,122].

Holographic microscopy offers an alternative approach that does not require fluorescent labelling. As in the fluorescence assay, one first functionalizes micrometre-scale probe beads with surface groups that bind specifically to targets of interest, such as virus particles, antibodies or other proteins. One then records holograms of individual particles and fits these holograms with an effective-sphere generative model. Fitting reveals binding-induced changes in the inferred parameters[123]. The observed shift in effective diameter, for example, can be related to the coverage of bound targets.

This approach allows both rapid fitting and high sensitivity. When the molecules bind, they increase the effective diameter of the beads by a few nanometres, a difference that the holographic microscope can detect[124]. The resulting fits are precise enough to isolate changes in population distributions as the target molecules bind, enabling applications such as fluorescence-free immunoassays[125,126], as shown in FIG. 6b,c.

The validity of the effective-medium approach has been assessed in simulations based on the discrete-dipole approximation[23,25,26,127]. This approximation treats an inhomogeneous object as a set of point dipoles and allows computation of the scattered field of arbitrarily shaped objects. These simulations also show that one should use a low-index material for the probe bead, relative to the refractive index of the molecular coatings, to observe the greatest shift in effective diameter after binding. Future experiments might therefore employ a silica probe bead, with refractive index $n_p \approx 1.4$, instead of polystyrene, with $n_p = 1.6$.

Characterizing industrial dispersions. For many applications involving industrial dispersions, evaluating the efficacy and safety of the product requires detecting and differentiating multiple species of particulate contaminates and measuring their relative concentrations in dispersion. Hologram microscopy combined with the effective-sphere analysis approach is especially well suited

a Data   Best fit (core–shell model)   3D rendering of filled vesicle

b Data   Best fit (Lorenz–Mie model)   3D rendering of effective sphere

c

d

to such applications. This method can analyse multiple particle species in wastewater or industrial slurries with high throughput[66,70,75]. In these applications, contaminants or large aggregates appear as outliers in the continuous, real-time analysis of particle size and composition.

This method also has applications in the monitoring and development of biopharmaceuticals. The active ingredients of these complex medicines are proteins that can aggregate, compromising the medicine's effectiveness and, potentially, causing harmful immune response. Winters et al.[66] used holographic microscopy and an effective-sphere model to successfully differentiate multiple components of a model biopharmaceutical formulation, including silicone–oil emulsion droplets,

◀ Fig. 6 | **Property estimation and characterization. a** | Hologram of a vesicle encapsulating ~500 mM sucrose, alongside the best-fit hologram from a core–shell model and a 3D rendering of the best-fit vesicle, shown with a cut-away of the enclosed fluid. **b** | Hologram of a spherical bead that binds target molecules, alongside a best-fit hologram from an effective-sphere model, which treats the substrate bead and molecular layers as a single homogeneous sphere. The fit defines the effective diameter and effective refractive index (right). **c** | Results from the effective-sphere analysis for avidin binding to biotinylated polystyrene spheres. Plots show the distributions of inferred particle diameters $\rho(d_p)$ and refractive indexes $\rho(n_p)$ from control beads (blue), probe beads after binding (red) and differences. Binding causes a statistically significant shift in $\rho(d_p)$ in the order of a few nanometres. **d** | Inferred parameters for a heterogeneous, four-particle mixture from a generative modelling approach (left), a machine-learning approach (middle) and a hybrid approach (right). The results show how well each method differentiates components of the mixture, which contains two sizes each of polystyrene and silica spheres. Ovals mark 99% confidence intervals of the generative modelling results. Colour denotes the relative probability density of the parameters, $P(d_p, n_p)$. Part **a** adapted with permission from REF.[120], A. Wang. Parts **b** and **c** adapted with permission from REF.[125], Optica Publishing Group. Part **d** adapted with permission from REF.[50], ACS.

fatty-acid clusters and potentially dangerous protein aggregates. Although many of these populations have a wide polydispersity in size, they can be distinguished by their common refractive index, indicating their similar composition. Characterizing the particles' size and composition differentiates the populations of these different species with high throughput and allows their concentrations to be measured accurately. Monitoring the concentration and composition of particles dispersed in biopharmaceutical products is useful for guiding product formulation, performing quality assurance during manufacturing and assessing product stability.

Reproducibility and data deposition

Reproducible, quantitative analysis with holographic microscopy requires recording and disclosing experimental metadata, storing large data sets and reporting the prior probabilities and techniques used in the analysis. The metadata are essential for interpreting recorded holograms. Metadata include both laser settings — such as wavelength, polarization and intensity — and imaging settings — such as pixel spacing, frame rate and exposure time. To determine the pixel spacing, we image a graticule, and then divide the distance between markings by the number of pixels spanning that distance. We recommend recording all metadata in the same file as the hologram and maintaining these metadata throughout hologram processing and analysis. Both HDF5 and TIFF files support storing metadata alongside data.

Some video recording formats are unsuitable for quantitative holographic imaging because they use lossy encoding to reduce file size. Lossy formats introduce artefacts into recorded images that can alter extracted results. The data should instead be saved as an uncompressed video or in a format that uses lossless compression, such as HDF5 or TIFF.

To store a time series of recorded holograms, which has a size typically in the order of gigabytes, we recommend using standard, non-proprietary formats such as HDF5. HDF5 has several advantageous features for holography: it is designed for large data sets, it can store data in a compressed format and implementations such as the h5py Python package enable HDF5 files to be loaded piecewise, so that they do not consume all of the computer's RAM.

Polydispersity
The distribution of sizes within a sample.

Graticule
A set of parallel lines with known spacing used for measuring scale.

Lossy encoding
Methods of compressing or transferring data that approximate or down-sample the data.

Equally important to experimental metadata are parameters associated with hologram analysis. It is essential to disclose all assumptions, including the generative model and the prior probabilities, which are probability distributions in a Bayesian analysis but could also take the form of bounds placed on parameters. Algorithmic parameters should also be disclosed, such as the convergence criteria for non-linear least-squares fitting, the number of chains for MCMC sampling or the number of temperatures for parallel tempered MCMC sampling. In a machine-learning framework, the underlying algorithm architecture and the training data should be reported. One can disclose all of this information by creating public repositories for both data and analysis code.

Limitations and optimizations

Limits on the information that can be inferred from holograms are both physical and practical. The physical limitations do not depend on the analysis technique used. They are based on how much information is present in the hologram. For example, when the particle approaches within roughly 5 μm of the focal plane of the objective, the fringes in its hologram become too finely spaced for the camera to resolve[37,77]. Conversely, when the particle moves too far from the focal plane, its fringes become increasingly faint and are obscured by image noise. Even under ideal imaging conditions, some combinations of particle parameters produce nearly indistinguishable holograms, which can lead to unreliable parameter estimation[128]. Furthermore, weakly scattering objects introduce degeneracies in the generative model, making it difficult to determine, for example, the size and refractive index of the object independently. In these cases, a Bayesian inference approach with a generative model will report appropriately larger uncertainties. Finally, the presence of many objects in the specimen can make it more difficult to extract information from the hologram, because fringes from other objects disrupt the fringes of interest. Machine-learning methods can be used to isolate clean holograms of the object of interest[129].

Generative modelling. The main practical limitation of the generative modelling approach is that one must know what one is looking at before modelling it, a limitation not faced by reconstruction-based analyses. More specifically, the generative model must accurately describe the shape, structure and composition of the specimen. It must also accurately describe how its hologram is formed. Ignoring physical effects, such as strong aberrations, leads to systematic characterization errors[37]. Additional parameters in the model, such as the field rescaling parameter α, can improve the fit but may be difficult to interpret. Furthermore, even in the most complex models, the inferred parameters can depend on the distance between the object and the focal plane. Martin et al.[37] found that when the particle was closer than about 10 μm to the focal plane, the inferred refractive index of the particle had a variation of 6%, whereas the inferred diameter had a variation as high as 20%. Such results may indicate that the model does not

account for some physical effects. To overcome these limitations, future work should focus on more descriptive and accurate generative models.

Another practical limitation is the computational cost of fitting. Fitting the more complex generative models, such as those describing the scattering from a cluster of many spherical particles, can take hours of CPU (central processing unit) time for a single hologram. By contrast, the hologram of a single sphere can be computed in under a millisecond on a desktop computer. The computational cost of detailed analysis may be prohibitive for certain experiments, such as those involving long time series or high throughput.

New developments in computing and inference could mitigate these issues. For example, algorithms such as automatic differentiation[130,131], variational inference[132] and Hamiltonian Monte Carlo[81] can accelerate fitting models with large numbers of parameters. Additionally, graphics processing unit (GPU) and tensor processing unit (TPU) computing frameworks can parallelize the fitting of highly complex models to time series[133].

An alternative is to develop simpler models rather than more complex ones. The effective-sphere model is an example of a model that makes simplifying yet accurate physical approximations. This approach can reduce the burden of specifying the detailed shape and structure of the object, and can sharply reduce the computational cost. The challenge is to determine the appropriate approximation for the problem. To this end, one can test the approximations by running full scattering calculations using tools such as the discrete-dipole method[26].

Machine learning. Although machine-learning algorithms can perform more robustly over a wider parameter space than conventional algorithms, they can be inaccurate when their inputs differ too drastically from their training data. Imprecision in the localization algorithm, which estimates the position and extents of holograms, can also propagate uncertainty into parameters such as size and axial position[50].

The machine-learning approach is also limited by computational speed, although in a different way from the generative modelling approach. In particular, analysing data is fast, but training can be slow because many holograms must be generated to span the parameter space. Altman and Grier[50] achieved reliable results with a training set of 10^4 images, but in the theoretical limit 10^9 images would be required to achieve the parts per thousand precision of a generative modelling approach. Because the training data can be generated and labelled automatically, achieving high-precision classification is not an intractable problem for spherical specimens. Advances in network architecture and training protocols for high-precision tracking and characterization of spherical particles may soon be practical even with modestly sized training sets. But for non-spherical specimens, which include additional degrees of freedom such as shape and orientation, it may be impractical to generate and process enough training data for accurate characterization.

Using synthetic data to train machine-learning models has some disadvantages. Experimental artefacts, such as pattern noise in the camera, can significantly compromise accuracy. To mitigate this problem, one can either improve the experimental design or modify the models used to generate the training data. For example, one can measure the camera noise and incorporate it into the generated holograms[90], or generate the training data using models that more accurately describe the artefacts of the experimental system.

Hybrid approaches. A hybrid approach can, in principle, overcome the limitations of both the generative modelling and machine-learning approach. It removes the need for human input or prior knowledge, while benefiting from the speed of machine learning and precision of fitting. Nevertheless, the hybrid approach comes with caveats. First, it remains computationally expensive because the generated training data must span the parameter space. Second, fitting the model requires calculating many holograms, although we expect fitting times to be reduced if the machine-learning stage provides a good initial guess. Third, any fundamental inaccuracies and limitations in the generative model affect the analysis in both stages. In the machine-learning stage, these inaccuracies affect the training data and, therefore, the parameter estimates. The inaccuracies in these estimates can propagate to the results of the fitting stage, as the accuracy of the fit can depend on the starting point in parameter space.

More general limitations. It is difficult to know whether the model-based approach and in-line experimental geometry will be effective for a specimen that differs from the previous examples, or whether a different analysis or experimental technique could reveal more information. We cannot give specific information on the ranges of specimen concentration, size, shape or structure for which the approach will yield useful results. New studies are needed to probe the physical and practical limitations of analysing more complex specimens.

For those interested in using the approach but unsure whether it will work on a particular specimen, our advice is to try it. The in-line geometry is straightforward to set up, and open-source software for generative modelling[83] and machine learning[50] makes it easy to apply the analysis methods.

Outlook

Since its development in the 1940s, holographic microscopy has been repeatedly revitalized by technological developments. The invention of the laser simplified implementation[134]; the development of digital cameras enabled digital reconstruction[135]; and the advent of computers powerful enough to compute scattering solutions of microscopic objects enabled direct analysis of holograms[136,137]. Recent developments in statistical inference and machine learning enabled the model-based approaches and precise measurements discussed in this Primer.

The future of model-based analysis depends on continued advances in inference and computation. Removing limitations, such as the variation of parameter estimates with defocus, demands more physically accurate

generative models. These models must also be more computationally efficient. Currently, it takes days of CPU time to fit a complex generative model to a hologram of a two-sphere cluster if the model includes the effects of a lens[78]. Although processing power will likely increase, there is still a need for numerical and algorithmic optimization. Real-time analysis of holograms requires inference algorithms that are more efficient. These algorithms must also be resilient to the complications of real experimental systems, such as variations in brightness and loss of fringe information near the focal plane.

Machine-learning techniques are poised to meet many of these challenges. CNNs have quantified the properties of microscopic objects from real holograms taken under various experimental conditions, at speeds nearly 100 times faster than conventional inference-based techniques. However, these property estimates are not as precise as those obtained with a fitting approach, and they lack the uncertainty estimates provided by MCMC sampling. Furthermore, estimating properties such as the shape, structure and orientation of more complex specimens requires algorithms trained with a large amount of data. Machine-learning approaches rely on generative models to produce these training data. The future of the field will likely depend on the development of both approaches in parallel.

We would go further; we think the future of holographic microscopy depends not only on the parallel development of generative modelling and machine learning but on their integration. We envision a microscope that would send its holograms directly to a system that could guess what kind of objects made them, analyse the holograms and report any parameters and uncertainties that the researcher specifies. The specimen might be a living eukaryotic cell, and the objects might be its organelles. Behind the scenes, a hybrid approach would be at work. A machine-learning module would determine the number, shapes and structures of objects

that made the hologram; estimate the properties of these objects; and select a generative model for each. A fitting module would then report precise estimates and marginalized uncertainties on parameters of interest, using the results from the machine-learning module as initial estimates.

The development of these new algorithms could be synergistic with experimental design. In the broad field of quantitative phase microscopy[14,138–140], researchers leverage various experimental approaches — off-axis beam geometries, phase-shifting elements, coherence control and multi-wavelength apparatus, among others — to acquire more information and more sensitive measurements of complex specimens. Meanwhile, interferometric scattering techniques have pushed the detection limit of holographic microscopy to the single-molecule scale[141,142]. Generative models are starting to appear for these techniques[143]. The development of generative modelling and machine-learning approaches could drive further advances in experimental techniques, and vice versa.

This vision is not limited to holographic microscopy; it is a vision for where microscopy in general may be headed. As we noted in the Introduction, a hologram is not easy for the human eye to interpret. It is difficult to visually recognize even a specimen's shape from its hologram, let alone its size or orientation. But the interference fringes that make the hologram impenetrable to human vision contain a wealth of information about the specimen. That information is most easily extracted and quantified by an algorithm. The same principle can be applied to any microscopy technique. By removing the need for humans to directly interpret the image, we can design microscopes that maximize the amount of information contained in the image. Although the resulting images may not appeal to the eye, their true appeal lies in what they reveal about the specimen.

Published online: 20 October 2022

1. Sheng, J., Malkiel, E. & Katz, J. Digital holographic microscope for measuring three-dimensional particle distributions and motions. *Appl. Opt.* **45**, 3893–3901 (2006).
2. Gabor, D. A new microscopic principle. *Nature* **161**, 777–778 (1948).
3. Gabor, D. & Bragg, W. L. Microscopy by reconstructed wave-fronts. *P. Roy. Soc. Lond. A Mat.* **197**, 454–487 (1949).
   Together with Gabor (1948), this paper demonstrates that it is possible to optically reconstruct a 3D representation of a specimen from its recorded hologram, a finding that launched the field of holographic microscopy.
4. Xu, W., Jericho, M. H., Meinertzhagen, I. A. & Kreuzer, H. J. Digital in-line holography for biological applications. *Proc. Natl Acad. Sci. USA* **98**, 11301–11305 (2001).
5. Xu, W., Jericho, M. H., Kreuzer, H. J. & Meinertzhagen, I. A. Tracking particles in four dimensions with in-line holographic microscopy. *Opt. Lett.* **28**, 164–166 (2003).
6. Berg, M. J. Tutorial: Aerosol characterization with digital in-line holography. *J. Aerosol Sci.* **165**, 106023 (2022).
7. Kim, M. K. Principles and techniques of digital holographic microscopy. *SPIE Rev.* **1**, 018005 (2010).
8. Jericho, S. K., Garcia-Sucerquia, J., Xu, W., Jericho, M. H. & Kreuzer, H. J. Submersible digital in-line holographic microscope. *Rev. Sci. Instrum.* **77**, 043706 (2006).
9. Garcia-Sucerquia, J. et al. Digital in-line holographic microscopy. *Appl. Opt.* **45**, 836–850 (2006).
10. Bishara, W., Zhu, H. & Ozcan, A. Holographic optofluidic microscopy. *Opt. Express* **18**, 27499–27510 (2010).
11. Marquet, P. et al. Digital holographic microscopy: a noninvasive contrast imaging technique allowing quantitative visualization of living cells with subwavelength axial accuracy. *Opt. Lett.* **30**, 468–470 (2005).
12. Mölder, A. et al. Non-invasive, label-free cell counting and quantitative analysis of adherent cells using digital holography. *J. Microsc.* **232**, 240–247 (2008).
13. Kemper, B. & Bally, G. V. Digital holographic microscopy for live cell applications and technical inspection. *Appl. Opt.* **47**, A52–A61 (2008).
14. Park, Y., Depeursinge, C. & Popescu, G. Quantitative phase imaging in biomedicine. *Nat. Photonics* **12**, 578–589 (2018).
15. Barty, A., Nugent, K. A., Roberts, A. & Paganin, D. Quantitative phase tomography. *Opt. Comm.* **175**, 329–336 (2000).
16. Popescu, G. *Quantitative Phase Imaging of Cells and Tissues* (McGraw-Hill Education, 2011).
17. Popescu, G. et al. Imaging red blood cell dynamics by quantitative phase microscopy. *Blood Cell Mol. Dis.* **41**, 10–16 (2008).
18. Marquet, P., Depeursinge, C. & Magistretti, P. J. Review of quantitative phase-digital holographic microscopy: promising novel imaging technique to resolve neuronal network activity and identify cellular biomarkers of psychiatric disorders. *Neurophotonics* **1**, 020901 (2014).
19. Mie, G. Beiträge zur Optik trüber Medien, speziell kolloidaler Metallösungen [German]. *Ann. Phys.* **330**, 377–445 (1908).
20. Ovryn, B. & Izen, S. H. Imaging of transparent spheres through a planar interface using a high-numerical-aperture optical microscope. *JOSA* **17**, 1202–1213 (2000).
   The authors fit a generative model based on Lorenz–Mie theory to a recorded hologram to determine the properties of a microscopic particle.
21. Lee, S.-H. et al. Characterizing and tracking single colloidal particles with video holographic microscopy. *Opt. Express* **15**, 18275–18282 (2007).
   This paper presents a straightforward generative model for hologram formation from a simple sphere, which has become the basis for many later studies on various systems.
22. Wang, A., Rogers, W. B. & Manoharan, V. N. Effects of contact-line pinning on the adsorption of nonspherical colloids at liquid interfaces. *Phys. Rev. Lett.* **119**, 108004 (2017).
23. Wang, A. et al. Using the discrete dipole approximation and holographic microscopy to measure rotational dynamics of non-spherical colloidal particles. *J. Quant. Spectrosc. Radiat. Transf.* **146**, 499–509 (2014).
24. Fung, J. et al. Measuring translational, rotational, and vibrational dynamics in colloids with digital holographic microscopy. *Opt. Express* **19**, 8051 (2011).
25. Yurkin, M. A. & Hoekstra, A. G. The discrete dipole approximation: an overview and recent developments. *J. Quant. Spectrosc. Radiat. Transf.* **106**, 558–589 (2007).

26. Yurkin, M. A. & Hoekstra, A. G. The discrete-dipole-approximation code ADDA: capabilities and known limitations. *J. Quant. Spectrosc. Radiat. Transf.* **112**, 2234–2247 (2011).

27. Pu, Y. & Meng, H. Intrinsic aberrations due to Mie scattering in particle holography. *J. Opt. Soc. Am. A* **20**, 1920 (2003).

28. Dulin, D., Barland, S., Hachair, X. & Pedaci, F. Efficient illumination for microsecond tracking microscopy. *PLoS ONE* **9**, e107335 (2014).

29. Giuliano, C. B., Zhang, R. & Wilson, L. G. Digital inline holographic microscopy (DIHM) of weakly-scattering subjects. *J. Vis. Exp.* **84**, e50488 (2014).

30. Kanka, M., Riesenberg, R., Petruck, P. & Graulig, C. High resolution (NA = 0.8) in lensless in-line holographic microscopy with glass sample carriers. *Opt. Lett.* **36**, 3651–3653 (2011).

31. Garcia-Sucerquia, J. Noise reduction in digital lensless holographic microscopy by engineering the light from a light-emitting diode. *Appl. Opt.* **52**, A232–A239 (2013).

32. Hell, S., Reiner, G., Cremer, C. & Stelzer, E. H. K. Aberrations in confocal fluorescence microscopy induced by mismatches in refractive index. *J. Microsc.* **169**, 391–405 (1993).

33. Wu, Y. & Ozcan, A. Lensless digital holographic microscopy and its applications in biomedicine and environmental monitoring. *Methods* **136**, 4–16 (2018).

34. Deng, N.-N. et al. Simple and cheap microfluidic devices for the preparation of monodisperse emulsions. *Lab. Chip* **11**, 3963–3969 (2011).

35. Kaz, D. M., McGorty, R., Mani, M., Brenner, M. P. & Manoharan, V. N. Physical ageing of the contact line on colloidal particles at liquid interfaces. *Nat. Mater.* **11**, 138–142 (2012).
This application of a generative modelling approach demonstrates the usefulness of the method: the fast, precise measurements enabled by the approach reveal a previously indiscernible phenomenon.

36. Moyses, H. W., Krishnatreya, B. J. & Grier, D. G. Robustness of Lorenz–Mie microscopy against defects in illumination. *Opt. Express* **21**, 5968 (2013).

37. Martin, C., Leahy, B. & Manoharan, V. N. Improving holographic particle characterization by modeling spherical aberration. *Opt. Express* **29**, 18212 (2021).

38. Fung, J., Perry, R. W., Dimiduk, T. G. & Manoharan, V. N. Imaging multiple colloidal particles by fitting electromagnetic scattering solutions to digital holograms. *J. Quant. Spectrosc. Radiat. Transf.* **113**, 2482–2489 (2012).

39. Cheong, F. C. et al. Flow visualization and flow cytometry with holographic video microscopy. *Opt. Express* **17**, 13071 (2009).

40. Dixon, L., Cheong, F. C. & Grier, D. G. Holographic particle-streak velocimetry. *Opt. Express* **19**, 4393–4398 (2011).

41. Edelstein, A. D. et al. Advanced methods of microscope control using μManager software. *J. Biol. Methods* **1**, e10 (2014).

42. Vercruysse, D. et al. Three-part differential of unlabeled leukocytes with a compact lens-free imaging flow cytometer. *Lab Chip* **15**, 1123–1132 (2015).

43. Dimiduk, T. G. et al. A simple, inexpensive holographic microscope. in *Biomedical Optics and 3-D Imaging, OSA Technical Digest (CD)* JMA38 (Optica, 2010).

44. Fung, J. *Measuring the 3D Dynamics of Multiple Colloidal Particles with Digital Holographic Microscopy*. PhD Thesis, Harvard Univ. (2013).

45. Moreno, D., Santoyo, F. M., Guerrero, J. A. & Funes-Gallanzi, M. Particle positioning from charge-coupled device images by the generalized Lorenz–Mie theory and comparison with experiment. *Appl. Opt.* **39**, 5117–5124 (2000).

46. Denis, L., Fournier, C., Fournel, T., Ducottet, C. & Jeulin, D. Direct extraction of the mean particle size from a digital hologram. *Appl. Opt.* **45**, 944–952 (2006).

47. Guerrero-Viramontes, J. A., Moreno-Hernández, D., Mendoza-Santoyo, F. & Funes-Gallanzi, M. 3D particle positioning from CCD images using the generalized Lorenz–Mie and Huygens–Fresnel theories. *Meas. Sci. Technol.* **17**, 2328–2334 (2006).

48. Yevick, A., Hannel, M. & Grier, D. G. Machine-learning approach to holographic particle characterization. *Opt. Express* **22**, 26884 (2014).
This paper is one of the first applications of machine learning to hologram analysis, and demonstrates the increase in speed of analysis that is possible.

49. Hannel, M. D., Abdulali, A., O'Brien, M. & Grier, D. G. Machine-learning techniques for fast and accurate feature localization in holograms of colloidal particles. *Opt. Express* **26**, 15221 (2018).

50. Altman, L. E. & Grier, D. G. CATCH: characterizing and tracking colloids holographically using deep neural networks. *J. Phys. Chem. B* **124**, 1602–1610 (2020).
This paper demonstrates a fully integrated pipeline for analysis of holograms, with improved automation and precision made possible by combining machine learning with fitting.

51. Hannel, M., Middleton, C. & Grier, D. G. Holographic characterization of imperfect colloidal spheres. *Appl. Phys. Lett.* **107**, 141905 (2015).

52. Duda, R. O. & Hart, P. E. Use of the Hough transformation to detect lines and curves in pictures. *Commun. ACM* **15**, 11–15 (1972).

53. Ballard, D. H. Generalizing the Hough transform to detect arbitrary shapes. *Pattern Recogn.* **13**, 111–122 (1981).

54. Dimiduk, T. G., Perry, R. W., Fung, J. & Manoharan, V. N. Random-subset fitting of digital holograms for fast three-dimensional particle tracking [invited]. *Appl. Opt.* **53**, G177–G183 (2014).

55. Dimiduk, T. G. & Manoharan, V. N. Bayesian approach to analyzing holograms of colloidal particles. *Opt. Express* **24**, 24045 (2016).
This work demonstrates the use of a Bayesian inference framework for hologram analysis, which has lent several advantages over non-linear least-squares fitting routines, including the formal integration of prior information and MCMC calculation of the posterior over parameters.

56. Moré, J. J. in *Numerical Analysis* (ed. Watson, G. A.) 105–116 (Springer, 1978).

57. Cheong, F. C., Krishnatreya, B. J. & Grier, D. G. Strategies for three-dimensional particle tracking with holographic video microscopy. *Opt. Express* **18**, 13563 (2010).

58. Krishnatreya, B. J. et al. Measuring Boltzmann's constant through holographic video microscopy of a single colloidal sphere. *Am. J. Phys.* **82**, 23–31 (2014).

59. Wang, A., McGorty, R., Kaz, D. M. & Manoharan, V. N. Contact-line pinning controls how quickly colloidal particles equilibrate with liquid interfaces. *Soft Matter* **12**, 8958–8967 (2016).

60. Wang, A. et al. Before the breach: interactions between colloidal particles and liquid interfaces at nanoscale separations. *Phys. Rev. E* **100**, 042605 (2019).

61. Roichman, Y., Sun, B., Stolarski, A. & Grier, D. G. Influence of nonconservative optical forces on the dynamics of optically trapped colloidal spheres: the fountain of probability. *Phys. Rev. Lett.* **101**, 128301 (2008).

62. Sun, B., Lin, J., Darby, E., Grosberg, A. Y. & Grier, D. G. Brownian vortexes. *Phys. Rev. E* **80**, 010401 (2009).

63. O'Brien, M. J. & Grier, D. G. Above and beyond: holographic tracking of axial displacements in holographic optical tweezers. *Opt. Express* **27**, 25375 (2019).

64. Xiao, K. & Grier, D. G. Sorting colloidal particles into multiple channels with optical forces: prismatic optical fractionation. *Phys. Rev. E* **82**, 051407 (2010).

65. Xiao, K. & Grier, D. G. Multidimensional optical fractionation of colloidal particles with holographic verification. *Phys. Rev. Lett.* **104**, 028302 (2010).

66. Winters, A. et al. Quantitative differentiation of protein aggregates from other subvisible particles in viscous mixtures through holographic characterization. *J. Pharm. Sci.* **109**, 2405–2412 (2020).

67. Wang, C., Shpaisman, H., Hollingsworth, A. D. & Grier, D. G. Celebrating soft matter's 10th anniversary: monitoring colloidal growth with holographic microscopy. *Soft Matter* **11**, 1062–1066 (2015).

68. Shpaisman, H., Jyoti Krishnatreya, B. & Grier, D. G. Holographic microrefractometer. *Appl. Phys. Lett.* **101**, 091102 (2012).

69. Cheong, F. C., Duarte, S., Lee, S.-H. & Grier, D. G. Holographic microrheology of polysaccharides from *Streptococcus mutans* biofilms. *Rheol. Acta* **48**, 109–115 (2009).

70. Wang, C. et al. Holographic characterization of protein aggregates. *J. Pharm. Sci.* **105**, 1074–1085 (2016).

71. Fung, J. & Hoang, S. Computational assessment of an effective-sphere model for characterizing colloidal fractal aggregates with holographic microscopy. *J. Quant. Spectrosc. Radiat. Transf.* **236**, 106591 (2019).
This work demonstrates the range of validity of the effective-sphere model in hologram analysis, used widely in industrial applications.

72. Wang, C. et al. Holographic characterization of colloidal fractal aggregates. *Soft Matter* **12**, 8774–8780 (2016).

73. Altman, L. E., Quddus, R., Cheong, F. C. & Grier, D. G. Holographic characterization and tracking of colloidal dimers in the effective-sphere approximation. *Soft Matter* **17**, 2695–2703 (2021).

74. Philips, L. A. et al. Holographic characterization of contaminants in water: differentiation of suspended particles in heterogeneous dispersions. *Water Res.* **122**, 431–439 (2017).

75. Cheong, F. C. et al. Holographic characterization of colloidal particles in turbid media. *Appl. Phys. Lett.* **111**, 153702 (2017).

76. Mackowski, D. W. & Mishchenko, M. I. Calculation of the *T* matrix and the scattering matrix for ensembles of spheres. *J. Opt. Soc. Am. A* **13**, 2266–2278 (1996).

77. Leahy, B. et al. Large depth-of-field tracking of colloidal spheres in holographic microscopy by modeling the objective lens. *Opt. Express* **28**, 1061–1075 (2020).

78. Alexander, R., Leahy, B. & Manoharan, V. N. Precise measurements in digital holographic microscopy by modeling the optical train. *J. Appl. Phys.* **128**, 060902 (2020).
This review highlights the historic development of the generative modelling approach to holograms (the only review to our knowledge that does so) and discusses the current abilities and limitations of existing generative models.

79. Geyer, C. J. in *Handbook of Markov Chain Monte Carlo* (eds Brooks, S., Gelman, A., Jones, G. L. & Meng, X.-L.) 3–48 (Chapman & Hall/CRC, 2011).

80. Hansen, N. & Ostermeier, A. Adapting arbitrary normal mutation distributions in evolution strategies: the covariance matrix adaptation. in *Proc. IEEE Int. Conf. Evolutionary Computation* 312–317 https://doi.org/10.1109/ICEC.1996.542381 (1996).

81. Neal, R. M. in *Handbook of Markov Chain Monte Carlo* (eds. Brooks, S., Gelman, A, Jones, G L, & Meng, X L) 113–162 (Chapman & Hall/CRC Handbooks of Modern Statistical Methods, 2011).

82. Earl, D. J. & Deem, M. W. Parallel tempering: theory, applications, and new perspectives. *Phys. Chem. Chem. Phys.* **7**, 3910–3916 (2005).

83. Barkley, S. et al. Holographic microscopy with Python and HoloPy. *Comput. Sci. Eng.* **22**, 72–82 (2019).

84. Crocker, J. & Grier, D. Methods of digital video microscopy for colloidal studies. *J. Colloid Interf. Sci.* **179**, 298–310 (1996).

85. Krishnatreya, B. J. & Grier, D. G. Fast feature identification for holographic tracking: the orientation alignment transform. *Opt. Express* **22**, 12773 (2014).

86. Parthasarathy, R. Rapid, accurate particle tracking by calculation of radial symmetry centers. *Nat. Methods* **9**, 724–726 (2012).

87. Rotskoff, G. M. & Vanden-Eijnden, E. Trainability and accuracy of neural networks: an interacting particle system approach. Preprint at https://doi.org/10.48550/arXiv.1805.00915 (2018).

88. Newby, J. M., Schaefer, A. M., Lee, P. T., Forest, M. G. & Lai, S. K. Convolutional neural networks automate detection for tracking of submicron-scale particles in 2D and 3D. *Proc. Natl Acad. Sci. USA* **115**, 9026–9031 (2018).

89. Schneider, B., Dambre, J. & Bienstman, P. Fast particle characterization using digital holography and neural networks. *Appl. Opt.* **55**, 133 (2016).

90. Klein, E. *Structure and Dynamics of Colloidal Clusters*. PhD Thesis, Harvard Univ. (2019).

91. Kingma, D. P. & Ba, J. Adam: a method for stochastic optimization. Preprint at https://doi.org/10.48550/arXiv.1412.6980 (2014).

92. Bottou, L. in *Proc. COMPSTAT'2010* (eds Lechevallier, Y. & Saporta, G.) 177–186 (Physica-Verlag HD, 2010).

93. Glorot, X., Bordes, A. & Bengio, Y. in *Proc. Fourteenth Int. Conf. Artificial Intelligence and Statistics* Vol. 15 (eds Gordon, G., Dunson, D. & Dudík, M.) 315–323 (PMLR, 2011).

94. Redmon, J. & Farhadi, A. YOLOv3: an incremental improvement. Preprint at https://doi.org/10.48550/arXiv.1804.02767 (2018).

95. Meng, G., Arkus, N., Brenner, M. P. & Manoharan, V. N. The free-energy landscape of clusters of attractive hard spheres. *Science* **327**, 560–563 (2010).

96. Szegedy, C., Vanhoucke, V., Ioffe, S., Shlens, J. & Wojna, Z. Rethinking the inception architecture for computer vision. in *Proc. IEEE Conf. Computer Vision and Pattern Recognition (CVPR)* 2818–2826 (IEEE, 2016).

97. Pickering, S. U. Emulsions. *J. Chem. Soc. Trans.* **91**, 2001–2021 (1907).

98. Xiao, J., Li, Y. & Huang, Q. Recent advances on food-grade particles stabilized Pickering emulsions: fabrication, characterization and research trends. *Trends Food Sci. Tech.* **55**, 48–60 (2016).

99. Yoon, K. Y. et al. Core flooding of complex nanoscale colloidal dispersions for enhanced oil recovery by in situ formation of stable oil-in-water Pickering emulsions. *Energ. Fuels* **30**, 2628–2635 (2016).

100. Bhargava, A., Francis, A. V. & Biswas, A. K. Interfacial studies related to the recovery of mineral slimes in a water–hydrocarbon liquid-collector system. *J. Colloid Interf. Sci.* **64**, 214–227 (1978).

101. Aveyard, R., Binks, B. P. & Clint, J. H. Emulsions stabilised solely by colloidal particles. *Adv. Colloid Interfac.* **100–102**, 503–546 (2003).

102. Dinsmore, A. D. et al. Colloidosomes: selectively permeable capsules composed of colloidal particles. *Science* **298**, 1006–1009 (2002).

103. Rahmani, A. M., Wang, A., Manoharan, V. N. & Colosqui, C. E. Colloidal particle adsorption at liquid interfaces: capillary driven dynamics and thermally activated kinetics. *Soft Matter* **12**, 6365–6372 (2016).

104. Fung, J. & Manoharan, V. N. Holographic measurements of anisotropic three-dimensional diffusion of colloidal clusters. *Phys. Rev. E* **88**, 020302 (2013).

105. Perry, R. W., Meng, G., Dimiduk, T. G., Fung, J. & Manoharan, V. N. Real-space studies of the structure and dynamics of self-assembled colloidal clusters. *Faraday Discuss.* **159**, 211–234 (2013).

106. Zia, R. N. Active and passive microrheology: theory and simulation. *Annu. Rev. Fluid Mech.* **50**, 371–405 (2018).

107. Style, R. W. et al. Traction force microscopy in physics and biology. *Soft Matter* **10**, 4047–4055 (2014).

108. Cheong, F. C. & Grier, D. G. Rotational and translational diffusion of copper oxide nanorods measured with holographic video microscopy. *Opt. Express* **18**, 6555 (2010).

109. Makarchuk, S., Beyer, N., Gaiddon, C., Grange, W. & Hébraud, P. Holographic traction force microscopy. *Sci. Rep.* **8**, 3038 (2018).

110. Moerner, W. E. & Fromm, D. P. Methods of single-molecule fluorescence spectroscopy and microscopy. *Rev. Sci. Instrum.* **74**, 3597–3619 (2003).

111. Steelman, Z. A., Eldridge, W. J., Weintraub, J. B. & Wax, A. Is the nuclear refractive index lower than cytoplasm? Validation of phase measurements and implications for light scattering technologies. *J. Biophotonics* **10**, 1714–1722 (2017).

112. Liu, P. Y. et al. Real-time measurement of single bacterium's refractive index using optofluidic immersion refractometry. *Procedia Eng.* **87**, 356–359 (2014).

113. Molaei, M. & Sheng, J. Imaging bacterial 3D motion using digital in-line holographic microscopy and correlation-based de-noising algorithm. *Opt. Express* **22**, 32119 (2014).

114. Wang, A., Garmann, R. F. & Manoharan, V. N. Tracking *E. coli* runs and tumbles with scattering solutions and digital holographic microscopy. *Opt. Express* **24**, 23719–23725 (2016).

115. Bozzuto, G. & Molinari, A. Liposomes as nanomedical devices. *Int. J. Nanomed.* **10**, 975–999 (2015).

116. Deamer, D. The role of lipid membranes in life's origin. *Life* **7**, 5 (2017).

117. Schwille, P. & Diez, S. Synthetic biology of minimal systems. *Crit. Rev. Biochem. Mol.* **44**, 223–242 (2009).

118. Spustova, K., Köksal, E. S., Ainla, A. & Gözen, I. Subcompartmentalization and pseudo-division of model protocells. *Small* **17**, 2005320 (2021).

119. Wang, A., Chan Miller, C. & Szostak, J. W. Core-shell modeling of light scattering by vesicles: effect of size, contents, and lamellarity. *Biophys. J.* **116**, 659–669 (2019).

120. Tran, L. H. A. et al. Measuring vesicle loading with holographic microscopy. Preprint at https://doi.org/10.48550/arXiv.2204.13068 (2022).

121. Quinn, M. K. et al. How fluorescent labelling alters the solution behaviour of proteins. *Phys. Chem. Chem. Phys.* **17**, 31177–31187 (2015).

122. Hughes, L. D., Rawle, R. J. & Boxer, S. G. Choose your label wisely: water-soluble fluorophores often interact with lipid bilayers. *PLoS ONE* **9**, e87649 (2014).

123. Markel, V. Introduction to the Maxwell Garnett approximation: tutorial. *J. Opt. Soc. Am. A* **33**, 1244–1256 (2016).

124. Zagzag, Y., Soddu, M. F., Hollingsworth, A. D. & Grier, D. G. Holographic molecular binding assays. *Sci. Rep.* **10**, 1932 (2020).

125. Altman, L. E. & Grier, D. G. Interpreting holographic molecular binding assays with effective medium theory. *Biomed. Opt. Express* **11**, 5225 (2020).

126. Snyder, K., Quddus, R., Hollingsworth, A. D., Kirshenbaum, K. & Grier, D. G. Holographic immunoassays: direct detection of antibodies binding to colloidal spheres. *Soft Matter* **16**, 10180–10186 (2020).

127. Draine, B. T. The discrete-dipole approximation and its application to interstellar graphite grains. *Astrophys. J.* **333**, 848–872 (1988).

128. Ruffner, D. B., Cheong, F. C., Blusewicz, J. M. & Philips, L. A. Lifting degeneracy in holographic characterization of colloidal particles using multi-color imaging. *Opt. Express* **26**, 13239–13251 (2018).

129. Rawat, S., Wendoloski, J. & Wang, A. cGAN-assisted imaging through stationary scattering media. *Opt. Express* **30**, 18145–18155 (2022).

130. Abadi, M. et al. TensorFlow: large-scale machine learning on heterogeneous distributed systems. Preprint at https://doi.org/10.48550/arXiv.1603.04467 (2015).

131. Bradbury, J. et al. JAX: composable transformations of Python + NumPy programs. *GitHub* http://github.com/google/jax (2018).

132. Kucukelbir, A., Tran, D., Ranganath, R., Gelman, A. & Blei, D. M. Automatic differentiation variational inference. *J. Mach. Learn. Res.* **18**, 1–45 (2017).

133. Jouppi, N. P. et al. In-datacenter performance analysis of a Tensor Processing Unit. in *Proc. 44th Annual Int. Symp. Computer Architecture* 1–12 (Association for Computing Machinery, 2017).

134. Leith, E. N., Upatnieks, J. & Haines, K. A. Microscopy by wavefront reconstruction. *J. Opt. Soc. Am.* **55**, 981–986 (1965).

135. Schnars, U. & Jüptner, W. Direct recording of holograms by a CCD target and numerical reconstruction. *Appl. Opt.* **33**, 179–181 (1994). **This paper represents another major development in the field of holographic microscopy: the application of the digital camera, which allows holograms to be reconstructed numerically rather than optically**.

136. Hickling, R. Holography of liquid droplets. *J. Opt. Soc. Am.* **59**, 1334–1339 (1969).

137. Slimani, F., Grehan, G., Gouesbet, G. & Allano, D. Near-field Lorenz–Mie theory and its application to microholography. *Appl. Opt.* **23**, 4140–4148 (1984).

138. Trujillo, C., Castañeda, R., Piedrahita-Quintero, P. & Garcia-Sucerquia, J. Automatic full compensation of quantitative phase imaging in off-axis digital holographic microscopy. *Appl. Opt.* **55**, 10299–10306 (2016).

139. Popescu, G. et al. Fourier phase microscopy for investigation of biological structures and dynamics. *Opt. Lett.* **29**, 2503–2505 (2004).

140. Joo, C., Akkin, T., Cense, B., Park, B. H. & de. Boer, J. F. Spectral-domain optical coherence phase microscopy for quantitative phase-contrast imaging. *Opt. Lett.* **30**, 2131–2133 (2005).

141. Piliarik, M. & Sandoghdar, V. Direct optical sensing of single unlabelled proteins and super-resolution imaging of their binding sites. *Nat. Commun.* **5**, 1–8 (2014).

142. Young, G. et al. Quantitative mass imaging of single biological macromolecules. *Science* **360**, 423–427 (2018).

143. Mahmoodabadi, R. G. et al. Point spread function in interferometric scattering microscopy (iSCAT). Part I: aberrations in defocusing and axial localization. *Opt. Express* **28**, 25969–25988 (2020).

Author contributions

Introduction (C.M., L.E.A., S.R., A.W., D.G.G. and V.N.M.); Experimentation (C.M., L.E.A., S.R., A.W., D.G.G. and V.N.M.); Results (C.M., L.E.A., S.R., A.W., D.G.G. and V.N.M.); Applications (C.M., L.E.A., S.R., A.W., D.G.G. and V.N.M.); Reproducibility and data deposition (C.M., L.E.A., S.R., A.W., D.G.G. and V.N.M.); Limitations and optimizations (C.M., L.E.A., S.R., A.W., D.G.G. and V.N.M.); Outlook (C.M., L.E.A., S.R., A.W., D.G.G. and V.N.M.); Overview of the Primer (C.M., L.E.A., S.R., A.W., D.G.G. and V.N.M.).

Competing interests

D.G.G. is a founder of Spheryx, Inc., which manufactures instruments for holographic particle characterization. The remaining authors declare no competing interests.

Peer review information

Nature Reviews Methods Primers thanks Radim Chmelik; Laurence Wilson, who co-reviewed with Sam Matthews; and the other, anonymous, reviewer(s) for their contribution to the peer review of this work.

Publisher's note

Springer Nature remains neutral with regard to jurisdictional claims in published maps and institutional affiliations.

RELATED LINKS
CATCH: https://github.com/laltman2/CATCH
HDF5: https://www.hdfgroup.org/solutions/hdf5/
HoloPy: http://holopy.readthedocs.io/
pylorenzmie: https://github.com/davidgrier/pylorenzmie